remote sensing

MDPI

Article

Normalized Difference Vegetation Index as an Estimator for Abundance and Quality of Avian Herbivore Forage in Arctic Alaska

Kyle R. Hogrefe [1], Vijay P. Patil [1], Daniel R. Ruthrauff [1], Brandt W. Meixell [1], Michael E. Budde [2], Jerry W. Hupp [1] and David H. Ward [1,*]

[1] Alaska Science Center, U.S. Geological Survey, 4210 University Drive, Anchorage, AK 99508, USA; hogrefek@oregonstate.edu (K.R.H.); vpatil@usgs.gov (V.P.P.); druthrauff@usgs.gov (D.R.R.); bmeixell@usgs.gov (B.W.M.); jhupp@usgs.gov (J.W.H.)

[2] Earth Resources Observation and Science Center, U.S. Geological Survey, 47914 252nd Street, Sioux Falls, SD 57198, USA; mbudde@usgs.gov

* Correspondence: dward@usgs.gov; Tel.: +1-907-786-7097

Received: 29 September 2017; Accepted: 13 November 2017; Published: 29 November 2017

Abstract: Tools that can monitor biomass and nutritional quality of forage plants are needed to understand how arctic herbivores may respond to the rapidly changing environment at high latitudes. The Normalized Difference Vegetation Index (NDVI) has been widely used to assess changes in abundance and distribution of terrestrial vegetative communities. However, the efficacy of NDVI to measure seasonal changes in biomass and nutritional quality of forage plants in the Arctic remains largely un-evaluated at landscape and fine-scale levels. We modeled the relationships between NDVI and seasonal changes in aboveground biomass and nitrogen concentration in halophytic graminoids, a key food source for arctic-nesting geese. The model was calibrated based on data collected at one site and validated using data from another site. Effects of spatial scale on model accuracy were determined by comparing model predictions between NDVI derived from moderate resolution (250 × 250 m pixels) satellite data and high resolution (20 cm diameter area) handheld spectrometer data. NDVI derived from the handheld spectrometer was a superior estimator ($R^2 \geq 0.67$) of seasonal changes in aboveground biomass compared to satellite-derived NDVI ($R^2 \leq 0.40$). The addition of temperature and precipitation variables to the model for biomass improved fit, but provided minor gains in predictive power beyond that of the NDVI-only model. This model, however, was only a moderately accurate estimator of biomass in an ecologically-similar halophytic graminoid wetland located 100 km away, indicating the necessity for site-specific validation. In contrast to assessments of biomass, satellite-derived NDVI was a better estimator for the timing of peak percent of nitrogen than NDVI derived from the handheld spectrometer. We confirmed that the date when NDVI reached 50% of its seasonal maximum was a reasonable approximation of the period of peak spring vegetative green-up and peak percent nitrogen. This study demonstrates the importance of matching the scale of NDVI measurements to the vegetation properties of biomass and nitrogen phenology.

Keywords: Alaska; Arctic; *Carex subspathecea*; geese; biomass; halophytic graminoids; NDVI; nitrogen

1. Introduction

Along the approximately 800 km-long Arctic Coastal Plain of Alaska (ACP), a rapid rise in air temperatures over the last half century has been associated with a decreasing ice pack, thawing of the permafrost, and a significant shift in the productivity and species composition of plant communities [1–3]. These dynamic environmental changes complicate predictions of the future abundance and distributions of coastal plant communities as some may be lost to sea level rise and

erosion, whereas others may be transformed from freshwater to halophytic species through saltwater intrusion [4,5]. Tools that monitor changes in the abundance and quality of arctic landscapes are needed to evaluate how wildlife habitats may be altered [6].

Halophytic graminoid wetlands provide high quality foods that are important for the reproductive success of three migratory avian herbivores on the ACP, lesser snow geese (*Chen caerulescens caerulescens*; hereafter snow geese), greater white-fronted geese (*Anser albifrons frontalis*; hereafter white-fronted geese), and black brant (*Branta bernicla nigricans*; hereafter brant) [7,8]. These wetlands contain plants that are high in nitrogen, a critical nutrient for the rapid growth of goslings during the short arctic summers. Populations of all three goose species have increased on the ACP over the last 30 years [9–11]. The halophytic graminoid wetlands on the ACP are widely distributed, and to date, grazing by geese has had little effect on productivity of these wetlands, indicating that they can likely support further increases in goose populations [8]. Knowing how biomass and nutrient quality of forage plants varies seasonally and annually is necessary to predictlong-term outcomes for these migratory avian herbivores [7].

Field measurements of forage plant biomass and nutritional quality typically involve time-intensive sample collection, often by destructive means, and processing that requires significant commitment of funding and personnel. Thus, there is great value in alternative techniques that yield accurate measures of forage abundance and quality while reducing costs and effort. Remotely sensed vegetation indices are well established tools of wildlife research and management that can serve as proxies for landscape level changes in biomass and nutrient quality without the repeated destructive sampling of vegetation [12–16]. Of these indices, the Normalized Difference Vegetation Index (NDVI) is one of easiest to calculate, most commonly available and has been proven to be an effective tool for monitoring vegetative changes across a wide range of terrestrial ecosystems, including alpine and arctic tundra, grasslands, and temperate and tropical forests [14–20], see [21] for a review. The index is a simple ratio calculation of the red and near-infrared (NIR) reflectance bands that is sensitive to the reflected photosynthetically active radiation of plants [22,23]. NDVI is highly correlated with plant productivity ("greenness" [24]), and therefore, is a good estimator of changes in aboveground biomass [13,24–26], canopy cover, and structure [27–29] in plant communities. Because NDVI measures photosynthetic activity, it also correlates positively with chlorophyll content [30], and in turn, nitrogen levels in plants [31]. The relationship between NDVI and nitrogen content in plants, however, has largely been based on fine scale ground-based spectrometer readings of agricultural crops and few studies have tested the accuracy of the relationship using satellite-derived NDVI at the landscape level [21]. Nevertheless, seasonal threshold metrics developed from repeated (time-series) measurements of NDVI values at the same location have proven useful in predicting the timing of both the start of the growing season (green-up) [32,33] and peak nitrogen concentration in forage plants [13,34,35], which are key indicators for reproductive success in arctic-nesting geese and other herbivores.

Increasingly, satellite-derived NDVI has been used in the Arctic to assess vegetative change in biomass and quality across landscapes and broad-scale communities [18,34–38], but few studies have been validated with concurrent assessments of NDVI and field measurements at landscape and fine-scale levels. These assessments are important because satellite-derived NDVI is not without errors. Accurate assessments in the Arctic are particularly challenging because of the frequent cloud cover, moist soils, sparse vegetative communities, and numerous water bodies that are known to influence spectral reflectance and accuracy in NDVI [21,39]. NDVI is also affected by soil reflectance in sparsely vegetated areas leading to underestimations of biomass, while in densely vegetated areas, NDVI can be influenced by leaf closure of the canopy that may cause values to plateau even though biomass increases [17,22,39]. Peak nitrogen levels in plants generally occur early in the growing season when plant growth is most rapid. But in the Arctic, this is also the period when plant density is low and snow melt creates areas of standing water.

The relationships between NDVI and biomass and nitrogen appear to differ among plant communities [26,27]. Low ($\geq$1 km^2)- to moderate (30 to 250 m^2)-resolution satellite-derived NDVI may not accurately detect changes in vegetative biomass and nutrient quality occurring at finer scales. For example, Doiron et al. [35] found that satellite-derived NDVI with 1 km^2 pixels was a good estimator of peak nitrogen availability in arctic wet (freshwater) tundra plants but was a mediocre estimator for seasonal changes in biomass. NDVI is sensitive to scattering of red and NIR bands associated with atmospheric contaminants [40]. Therefore, it is important to validate the accuracy of NDVI as an estimator with empirical data in the environment of interest.

We used high resolution (20 cm diameter area) ground- and moderate resolution (250 $\times$ 250 m pixels) satellite-derived data to evaluate seasonal relationships between NDVI and field measures of biomass and nutritional quality of halophytic graminoids on the ACP. To the best of our knowledge this is the first study to assess the efficacy of moderate resolution satellite-derived NDVI as a predictor of biomass and quality in halophytic graminoid grazing lawns, where herbivory strongly influences plant structure and nutrient cycling [41]. We were particularly interested in determining whether NDVI could be used as an alternative to intensive species-level sampling. Our primary objectives were to: (1) model the relationships between NDVI and field measurements of aboveground biomass and nitrogen concentration in halophytic graminoid wetlands, and (2) assess whether the relative timing of peak nitrogen concentration in halophytic wetland plants could be identified based on NDVI. We compared NDVI-derived phenology as predictors of the date of peak nitrogen concentration. We explicitly determined the best predictor and validated our assessments with multi-year, site-specific collections, which differs from other studies in the Arctic. We also investigated the influence of environmental variables, spectral-band definitions, and spatial scale on seasonal NDVI predictions of biomass and nitrogen concentration. Finally, we tested the site-specificity of biomass predictions in a validation exercise involving halophytic graminoid wetlands in a similar ecosystem located approximately 100 km from our primary study site.

2. Study Area

We conducted our study between mid-May and mid-August, 2011–2015 at two sites along the coast of the central ACP, one in the Colville River Delta (CRD) and the other in the Smith River estuary near Point Lonely (PL; Figure 1). Our primary study site was the CRD, where we established the relationships between NDVI and plant biomass and nitrogen. We validated those relationships at the other study site (PL). Each site supported expanses of halophytic graminoid wetlands in low (<1 m above sea level) lying areas near (<3 km) the coast [42]. The plants within the halophytic graminoid wetlands were dominated by *Carex subspathacea* ($\geq$98%) that was interspersed with *Puccinellia* spp., *Stellaria* spp., and moss. The canopy height of the *C. subspathacea*-dominated wetlands remained short (<6 cm) during the study period, possibly because of repetitive grazing by geese. Intermixed among the stands of *C. subspathacea* and immediately adjacent and inland at higher elevations (>1 m) to the wetlands were polygonal ice-wedge ponds and lakes surrounded by freshwater graminoid wetlands dominated by *C. aquatilis* and *Eriophorum angustifolium* in the low lying moist areas and emergent species like *Arctophila fulva* and *Hippuris vulgaris* in the larger shallow ponds and lakes. Mixed communities of dwarf shrubs (e.g., *Salix ovalifolia*) and grasses (e.g., *Poa* spp.) occupied the rims of sloughs and elevated areas where soils were drier. Brant and snow geese nested coastally in elevated freshwater graminoid wetlands, mixed plant communities, and islands of lakes, while white-fronted geese were dispersed across inland (>3 km) locations; all three species foraged in the halophytic graminoid wetlands during nesting (June–July) and brood-rearing (July–August).

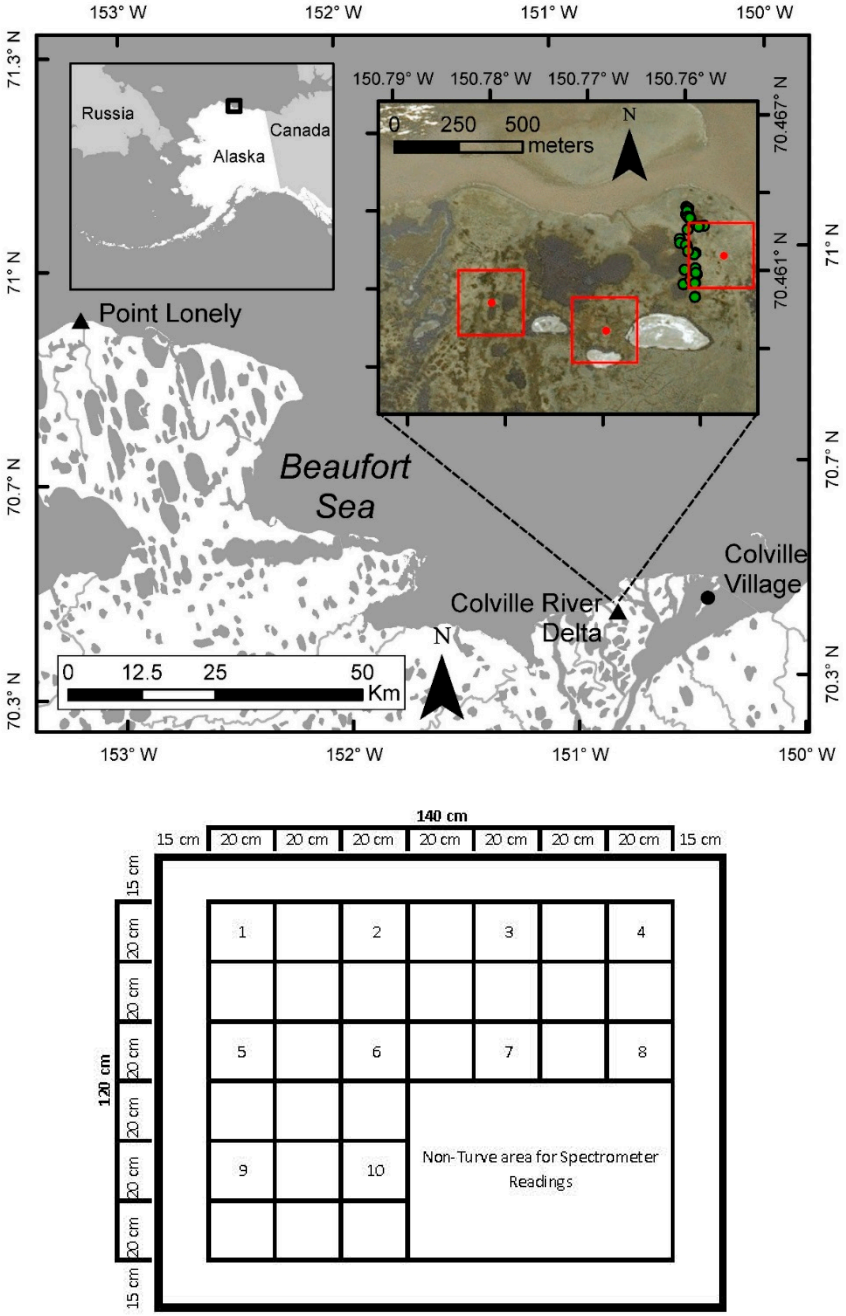

Figure 1. Study area locations on the Arctic Coastal Plain of Alaska (top; triangles) with insert (SPOT5 satellite imagery) showing orientation of vegetation plots (green points) in relation to three "expedited" Moderate Resolution Imaging Spectroradiometer (eMODIS) pixels (red; red dot = center) and schematic of plot layout (bottom) where biomass and percent nitrogen of halophytic graminoids were measured. High resolution measurements of Normalized Difference Vegetation Index (NDVI) were collected using a handheld spectrometer within each plot (see Methods).

3. Methods

3.1. Vegetation Sampling and Processing

Coinciding with snow melt in late May or early June, we setup paired exclosure/control plots within large (>1 km^2) *C. subspathacea*-dominated wetlands at both study sites. Within wetlands, we opportunistically located plots in relatively homogeneous patches of *C. subspathacea* that encompassed a broad range of variation in biomass. New plots were selected each year because

our sampling procedure potentially had carryover effects on biomass in subsequent years. We sampled 5–8 pairs of exclosure/control (i.e., ungrazed/grazed) plots (8–16 plots per year) between 2011 and 2015. We sampled both grazed and ungrazed plots to ensure that our measurements contained a representative range of potential variation in biomass and nitrogen composition. We also believed that any effects of grazing on biomass of *C. subspathacea* were minimal because within-year differences in average biomass ranged 5–22 g m^{-2} between grazed and ungrazed plots. The magnitude of biomass lost to grazing was, therefore, small relative to the observed range of inter-annual variation in biomass across samples (see below). Similarly, we found no evidence that nitrogen concentrations were substantially different between grazed and ungrazed plots; within-year differences in average percent nitrogen ranged 0.00–0.09%.

On intervals of 6–10 days, we randomly selected and removed a 20 × 20 cm turve (block of vegetation and soil) from each plot to a depth of approximately 5 cm, clipped and preserved all aboveground biomass, and then returned the substrate to the sample location. Turves were spaced 10–20 cm apart to prevent edge effect from previous sample collection and >10 cm away from the plot perimeter to avoid potential effects of the exclosure material on vegetative growth; a 50 × 50 cm sector of each plot was left undisturbed for NDVI sampling (Figure 1).

Processing and analysis of vegetation samples varied slightly between study sites. At the CRD, vegetation samples were rinsed in fresh water, dried at ambient temperature, and all live *C. subspathacea* and *Puccinellia* spp. were separated from other vegetation and frozen. After the field season, samples were dried to constant mass at 50 °C and weighed (g). A subsample (0.5–1.0 g) was analyzed for percent nitrogen using a C-N analyzer at the Washington State University Wildlife Habitat and Nutrition Laboratory. Vegetation samples at PL were clipped and rinsed as at the CRD, but then immediately dried at 50 °C for 48 h and stored; after the field season, samples were sorted and then dried to constant mass and weighed following the same methods as with the CRD samples. Differences in biomass between sorting methods was negligible when a set of turves (n = 9) was divided into equal sub-samples, clipped (early, mid, and late season), and then half sorted prior to drying and the other sorted after drying (Hogrefe unpublished data).

3.2. Environmental Data

At the CRD, we placed a sensor in the center of each exclosure to measure hourly soil temperature (±0.21 °C) at a depth of 6 cm. Sensors were placed in the ground just after thawing in early June each year and soil temperature was recorded across all sampling intervals. We obtained hourly precipitation data from the National Oceanic and Atmospheric Administration National Climate Data Center (www.ncdc.noaa.gov/cdo-web/) for Anachlik Island (Colville Village, 2011–2015; Figure 1), located 15 km east of the CRD site. Daily mean values of each environmental variable were converted to cumulative value to date, cumulative value per study period, and mean value per study period based on the sample interval for each field season.

3.3. NDVI Data

In association with vegetation sampling, we obtained hyperspectral reflectance profiles at each plot using handheld spectrometers manufactured by Unispec (Amesbury, MA, USA; at CRD) and Ocean Optics (Largo, FL, USA; at PL). Controlled trials comparing the two units across a range of halophytic graminoid densities demonstrated that the units measured essentially equal NDVI values (Figure A1). The spectrometers recorded reflectance profiles within a 20 cm diameter area at a spectral resolution of 3.2–3.4 nanometers (nm) and range of 301.6–1143.4 nm. The sensor optic was mounted on a 1.2 m-long fiber optic cable and had a 25° field of view, providing a ratio of sensor height to reading footprint diameter of approximately 2:1. Prior to each reflectance reading, spectrometers were calibrated against a white standard to normalize for any changes in light conditions between sampling occasions. Reflectance readings were taken from a height of 50 cm, centered on the selected turve and

the undisturbed sector (Figure 1). We used the turve reading to compare NDVI with biomass and nitrogen. A reading of undisturbed vegetation in the plot served as a control.

We calculated two separate NDVI values using reflectance readings from handheld spectrometers: one based on band definitions for the "expedited" Moderate Resolution Imaging Spectroradiometer (eMODIS) imagery from the Terra satellite [43], and the other based on band definitions for the WorldView-2 satellite imagery. The band definitions for eMODIS NDVI were red = 616–674 nm and near infrared (NIR) = 837–880 nm; for WorldView-2 NDVI, the definitions were red = 630–690 nm and NIR = 770–895 nm. Hereafter, the handheld spectrometer measurements based on these two sets of band definitions are referred to as SR_{eMO} and SR_{WV2}, respectively. Reflectance was derived as the mean of all hyperspectral values falling within each of the band ranges and NDVI was calculated as: NDVI = (NIR − Red)/(NIR + Red) [21].

We obtained satellite-derived eMODIS NDVI data for the halophytic graminoid wetlands at CRD and PL from the US Geological Survey-Earth Resources Observation and Science Center (USGS EROS). The eMODIS NDVI for Alaska is a 7–day maximum value composite dataset that provides consistent geographic and temporal coverage while accounting for atmospheric contamination [43,44]. The USGS EROS eMODIS NDVI data uses the MODIS L1B Terra surface reflectance data made available by the National Aeronautics and Space Administration (NASA) that is corrected for molecular scattering, ozone absorption, and aerosols. We also applied additional corrections for atmospheric effects using a temporal smoothing filter [45] to the time series data.

We acquired satellite-derived NDVI data for three, 250 × 250 m pixels that were positioned to minimize inclusion of water bodies while including halophytic graminoid wetlands near the paired exclosure/control plots (Figure 1). Stands of *C. subspathacea* comprised a significant portion, but not the majority, of the area of the eMODIS pixels. Excluding water, an eMODIS pixel comprised an average of approximately 40% *C. subspathacea*-dominated halophytic graminoids, 40% freshwater graminoids, 10% dwarf shrubs, and 10% unvegetated (sand/mud; Hogrefe unpublished data).

3.4. Analyses

3.4.1. Predicting Aboveground Biomass and Nitrogen Biomass Using NDVI

We followed an information-theoretic approach [46] to assess support for NDVI and environmental variables as predictors in analyses of aboveground biomass (g live *C. subspathacea* m^{-2}) and nitrogen biomass (g nitrogen m^{-2}) using data collected at the CRD. Our primary objectives were to determine the utility of NDVI in predicting our response variables and identify explanatory variables that may improve predictive power. We fitted generalized linear mixed-effects models to account for the effect of our plot-based sample design, with sample plots modeled as a random effect and other variables modeled as fixed effects [47]. To assess whether NDVI band definitions affected the accuracy of biomass predictions, we tested calculations of plot-level NDVI from handheld spectrometers (SR_{eMO} and SR_{WV2}) as separate variables. We also included a variable for landscape-level NDVI from satellite-based eMODIS (eMO) to assess the effect of spatial scale on model accuracy. Soil temperature and precipitation influence productivity of arctic tundra plants [29,48], so we considered the environmental variables cumulative degree days above 0 °C up until sample collection (temperature) and cumulative precipitation between sampling periods (precipitation). We also considered day of year (date) as a continuous variable to control for repeated sampling across the growing season. Because the intent of our approach was to derive a predictive model for future applications, we did not explicitly model the effect of year on our estimates of biomass. Because of differences in clipping techniques in 2011 from other years, we excluded 2011 vegetation samples from analyses of biomass, but retained them for analyses of nitrogen concentration. Values of temperature and biomass were $\log_{10}$-transformed to align with the underlying assumptions of linear regression. In each analysis, we tested a suite of 17 models; each model contained one of the three NDVI variables alone and in conjunction with date, temperature, precipitation, and their additive combinations.

We calculated model-averaged parameter and prediction estimates using Akaike weights w_i [46] and considered parameters to be biologically meaningful if their 95% confidence intervals did not overlap zero. We conducted all analyses in R version 3.1.2 [49], fit mixed-effects models using the lme4 package [50], averaged model outputs using the AICcmodavg package [51], and calculated model-specific prediction intervals using the merTools package [52]. Because the information-theoretic approach provides a measure of relative model fit that reflects only the explanatory variables in a particular model set, we also calculated marginal R^2 for the fixed effects of each model as a measure of absolute model fit following the approach of Nakagawa and Schielzeth [53] using the piecewiseSEM package [54].

To assess the difference in biomass estimates between models that included environmental variables and date with those that did not, we applied observed date-specific values of temperature and precipitation to yield model-averaged predictions of biomass. Comparisons between models were made using approaches implemented by Knowles and Frederick [52].

3.4.2. Validation: Prediction of Biomass

To assess model performance over a broader spatial scale, we applied a model relating NDVI to *C. subspathacea* biomass derived at the CRD in 2012–2015 to NDVI values and vegetation samples collected at PL in 2012–2013. Model performance was evaluated by comparing the slopes of the linear relationships between predicted and observed biomass values.

3.4.3. Phenology Metric: Linking Seasonal Phenology in NDVI and Percent Nitrogen

We also examined whether seasonal patterns in NDVI could be used to predict the relative timing of peak nitrogen concentration. Percent nitrogen varies seasonally in arctic vegetation as a function of plant growth rates, tissue allocation, and nutrient resorption at the end of the growing season, with the highest nitrogen concentrations typically found in rapidly-growing early season tissues [55]. Because NDVI reflects the amount of photosynthetically active, green vegetation, the timing and rate of change in early-season NDVI values is expected to be associated with seasonal trend in percent nitrogen [35].

We estimated three NDVI-derived phenology metrics for predicting the date of peak nitrogen concentration: (1) the date of maximum rate of increase in NDVI (max Δ), (2) the date when NDVI reached 50% of its seasonal maximum (50% max), and (3) the date of maximum NDVI (max). The date of maximum rate of increase in NDVI is associated with rapid early-season plant growth and has been previously used to assess forage nitrogen content and habitat selection for arctic herbivores in Alaska [34]. The date of 50% max is meant to serve as a computationally simple approximation of the date of max Δ [35], while the date of max NDVI reflects the peak of vegetation greenness.

We compared NDVI and nitrogen phenology using satellite-derived eMODIS-derived NDVI (eMO) and handheld spectrometer-derived NDVI with band definitions from eMODIS (SR_{eMO}) and WorldView-2 (SR_{WV2}). This suite of variables allowed us to assess the accuracy of NDVI to predict nitrogen phenology for each year (2011–2015) across different scales and spectral band definitions. Annual growth curves for eMO were based on the median NDVI value of 3 pixels for each sampling event over the season, whereas the annual growth curves for SR_{eMO} and SR_{WV2} were fit to all plot data at each sampling event over the season. We pooled data across plots when fitting curves to avoid pseudoreplication among plots exposed to the same growing environment. This choice was based on previous research indicating that nitrogen phenology is strongly regulated by synoptic weather patterns [48], and by preliminary analyses showing strong similarity in seasonal curves among plots.

3.4.4. Phenology Curve Fitting and Metric Estimation

We modeled seasonal trends in NDVI using both Gaussian and lognormal functions with day of year (DOY) as the independent variable, as well as a null (intercept only) model (Table A1). Gaussian and lognormal curves have been used to describe nitrogen seasonal trends in previous

work linking NDVI and nitrogen phenology [35]. Both NDVI and percent nitrogen typically show unimodal but asymmetric seasonal trends, increasing rapidly to a peak early in the growing season and declining slowly thereafter due to a combination of senescence, decomposition, and nutrient resorption [48,55]. We generated model-averaged predictions of all NDVI variables using Akaike's information criterion adjusted for sample size AIC_c [46].

After curve-fitting, we estimated phenology indices using curve predictions rather than raw data because field measurements were obtained at coarse intervals (6–10 days). The date of maximum NDVI and 50% maximum were then estimated by generating model-averaged NDVI predictions across the growing season. We estimated the first derivative of the curves using finite difference approximation to determine the date of maximum rate of change in NDVI because model-averaged curves could not be solved numerically. To ensure that these indices were not constrained by a late start to the field season, we predicted NDVI and percent nitrogen values from 24 May (~earliest observed date of breakup) to 31 August, regardless of the dates when field measurements began and ended.

In contrast to seasonal assessments of NDVI, we modeled seasonal trends in nitrogen using a third-order polynomial. Exploratory plots of seasonal trends in percent nitrogen revealed a notable late-season increase in most years, which could not have been captured by either the Gaussian or lognormal curves. Because we did not need to estimate the date of maximum change in nitrogen, we chose the curve that best fit the data. All curves were fit to seasonal NDVI and percent nitrogen data in R [49], using the minpack.lm package [56].

3.4.5. Assessing Predictive Power of Phenology Metrics

We compared NDVI and nitrogen phenology by regressing the date of maximum percent nitrogen against each phenology metric using estimates from 2011–2015. We assessed predictive power by regressing predicted dates of peak nitrogen from these models against observed values from vegetation samples. In addition to examining standard regression statistics (R^2, r), we evaluated predictive bias using regression slopes and mean residual values. We considered results to be statistically significant at $\alpha \leq 0.05$. Because we only collected NDVI readings and vegetation samples over two years at PL, we were not able to validate our models of inter-annual variation in the timing of peak nitrogen concentration using an external dataset.

4. Results

4.1. Predictions of Biomass and Nitrogen Biomass

We measured biomass of 355 vegetation samples from 2012–2015 at the CRD. Dry biomass ranged from 4.6 to 214.0 g m^{-2}; mean values were highest in 2013 (94.0 g m^{-2}) and lowest in 2012 (54.5 g m^{-2}). Biomass of *C. subspathacea* increased as the season progressed, peaking in late July and early August before declining slightly, a pattern generally reflected by plot-level NDVI values (Figure 2). The best-supported biomass model (w_i = 0.30) contained the predictor variables SR_{WV2}, precipitation, temperature, and date (Table 1). The two handheld spectrometer-derived NDVI measures were highly correlated (Pearson's correlation coefficients r $\geq$ 0.993) and explained similar proportions of variation (R^2 = 0.67–0.70; Table 1), but WorldView-2 NDVI band definitions were supported over eMODIS. Both of the measures derived from the spectrometer were supported over the satellite-derived eMODIS NDVI ($R^2 \leq 0.40$; Table 1). Model-averaged parameter estimates were 1.41 (1.22–1.60 95% CI) for SR_{WV2}, 1.47 (1.26–1.69 95% CI) for SR_{eMO}, and 0.77 (0.42–1.12 95% CI) for eMO. Whereas the variables precipitation, temperature, and date received support, their effects were minimal. The model-averaged predictions of biomass incorporating environmental variables averaged 1.85 g dry weight m^{-2} higher than those from the model using NDVI alone (Figure 3), and the prediction intervals of these two outputs largely overlapped.

Table 1. Model rankings and marginal R^2 for the relationship between NDVI, precipitation, temperature, date, and forage biomass of halophytic graminoids at the Colville River Delta, Alaska, 2012–2015. NDVI was derived from handheld spectrometers calculated at two band definitions (WorldView-2 (SR_{WV2}) and eMODIS (SR_{eMO})) and from eMODIS satellite (eMO). Precip = cumulative precipitation up to time of sampling, Temp = cumulative temperature up to time of sampling, and Date = Julian date. The number of parameters (k) includes +1k for an intercept, +1k for residual estimate, and +1k representing the random effect attributable to unique plots sampled repeatedly across a season.

Model	k	ΔAIC_c	w_i	Marginal R^2
SR_{WV2} + Precip + Temp + Date	7	0	0.30	0.67
SR_{WV2} + Precip + Date	6	0.52	0.23	0.68
SR_{WV2} + Temp + Date	6	0.65	0.22	0.67
SR_{WV2} + Date	5	0.74	0.21	0.67
SR_{eMO} + Precip + Temp + Date	7	5.95	0.02	0.68
SR_{eMO} + Temp + Date	6	6.08	0.01	0.68
SR_{WV2}	4	6.96	0.01	0.69
SR_{eMO} + Date	5	8.56	0	0.69
SR_{eMO} + Precip + Date	6	9.03	0	0.70
SR_{eMO}	4	13.66	0	0.70
eMO + Temp + Date	6	150.6	0	0.39
eMO + Precip + Temp + Date	7	151.18	0	0.40
Precip + Temp + Date	6	167.87	0	0.36
eMO + Date	5	177.69	0	0.38
eMO + Precip + Date	6	178.48	0	0.38
eMO	4	236.88	0	0.34
Intercept only	3	441.58	0	0.00
The lowest AIC_c score in the analysis was −416.47				

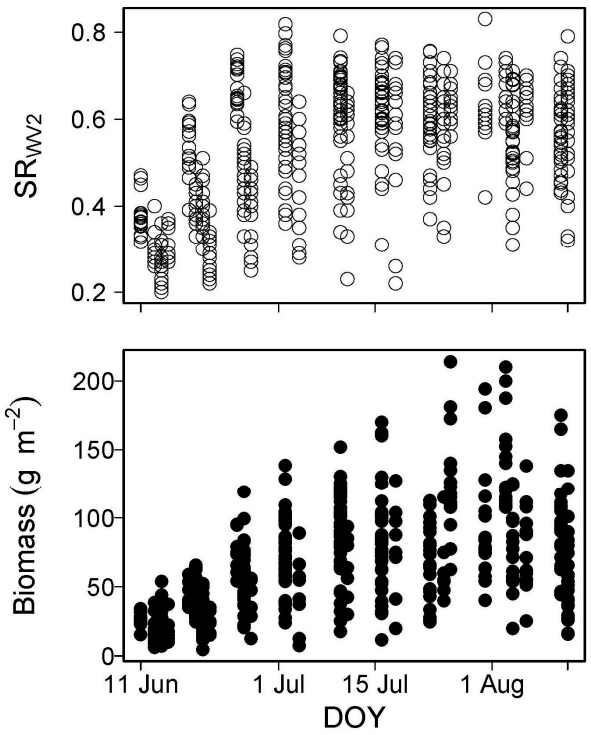

Figure 2. Biomass (g m^{-2}) of halophytic graminoids (filled symbols) and plot-level NDVI values (open symbols) by season date at the Colville River Delta, Alaska, 2012–2015. NDVI values plotted here were derived at WorldView-2 band definitions using a handheld spectrometer. Dates are representative of non-leap years (i.e., 2013–2015).

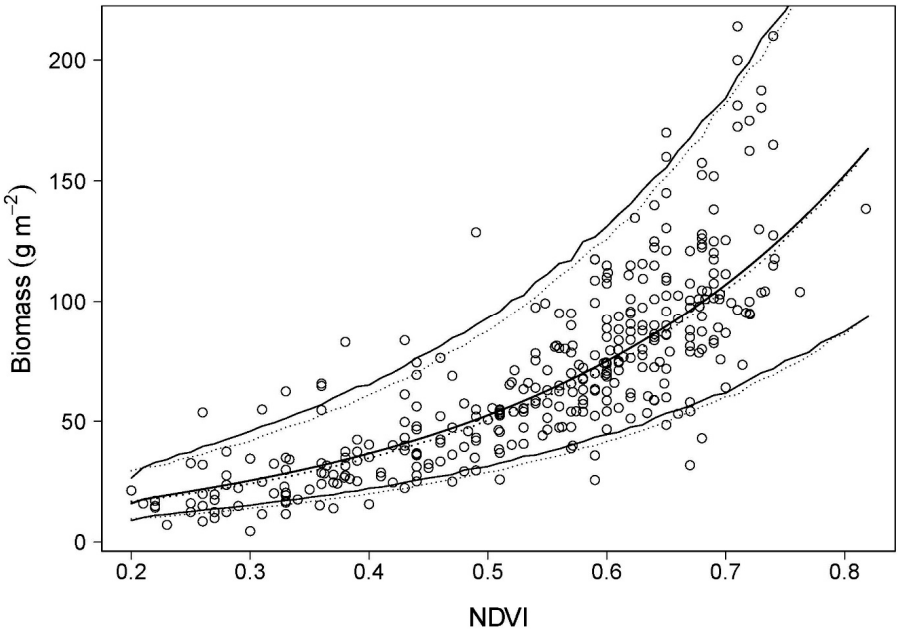

Figure 3. Relationship between graminoid biomass (g m^{-2}) and spectrometer-derived NDVI using WorldView-2 band definitions at the Colville River Delta, Alaska, 2012–2015. Open circles represent observed values. The bold solid line represents model-averaged predictions of biomass derived from a multi-model assessment with NDVI, temperature, precipitation, and date as predictor variables. The light solid lines depict the upper and lower 95% prediction intervals of the top-ranked model in Table 1, a close approximation of model-averaged predictions. The bold dashed line depicts predicted biomass as a function of spectrometer-derived WorldView-2 NDVI in the absence of environmental variables (i.e., the seventh-ranked model in Table 1), fitting the model $\log_{10}$(biomass) = 0.812 + 1.762(SR_{WV2}); the light dashed lines delimit the upper and lower 95% prediction intervals of this relationship.

We determined nitrogen concentration for 361 samples of *C. subspathacea* collected during 2012–2015 at the CRD. Nitrogen (% dry mass) ranged from 0.98% to 4.47%. Mean values were highest in 2014 (2.73%) and lowest in 2013 (2.15%). In contrast to biomass, percent nitrogen values generally peaked early in the season, decreased to a nadir in the first week of August, and increased slightly at the end of the season. Despite this pattern, values of nitrogen biomass essentially followed those of *C. subspathacea* biomass. Nitrogen and *C. subspathacea* biomass were highly correlated (Pearson's correlation coefficient r = 0.90), and our modeling efforts thus yielded similar results. Marginal R^2 values indicated that NDVI values derived by handheld spectrometer (R^2 0.61–0.66) explained more variance than satellite-derived eMODIS NDVI (R^2 0.55–0.57). Model rankings were nearly identical to those reported in Table 1, with spectrometer-derived WorldView-2 NDVI present in the top-ranked models (Σw_i = 1.00). Given the similarity of these findings to those detailed above for *C. subspathacea* biomass, modeling results are not shown.

4.2. Validation: Estimation of Biomass at PL Using Spectrometer-Derived NDVI

Because environmental variables added little predictive power, we used the NDVI-only, plot-based model derived at the CRD ($\log_{10}$(biomass) = 0.812 + 1.762(SR_{WV2})) to assess the accuracy of the relationship at a different location. Specifically, we applied this model to 242 spectrometer-derived NDVI values and associated vegetation biomass measurements from PL. Back-transformed predictions are plotted against observed values in Figure 4, a relationship described by the model $biomass_{observed}$ = 17.17 + 0.676($biomass_{predicted}$) ($F_{1, 240}$ = 512.5, $p < 0.01$, R^2 = 0.68). On average, the model relating NDVI to biomass determined at the CRD overestimated the observed

biomass at PL by 25%, with generally higher absolute errors at higher NDVI values (and hence, biomass; Figure 4).

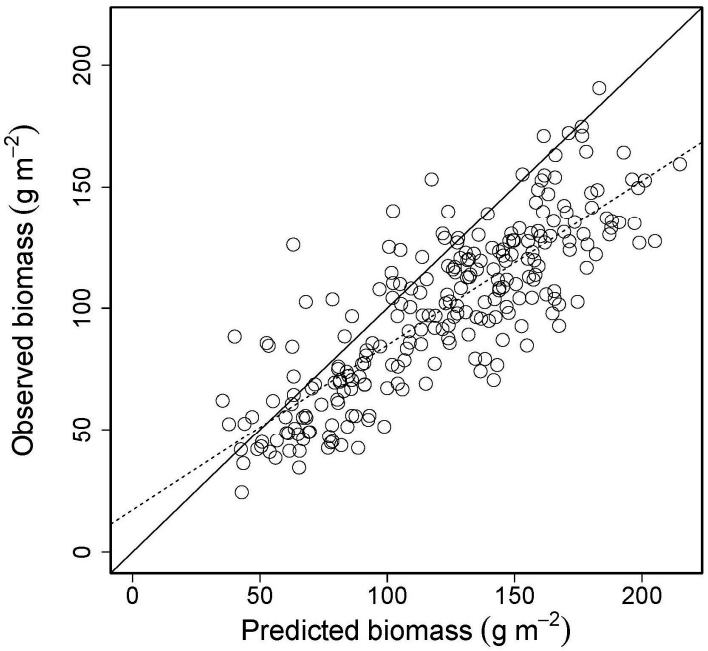

Figure 4. Relationship between observed biomass (g m^{-2}) of halophytic graminoids from Pt. Lonely, Alaska, 2012–2013, and the predicted biomass (g m^{-2}) based on the model $\log_{10}$(biomass) = 0.812 + 1.762(SR_{WV2}) where NDVI values were derived at WorldView-2 (SR_{WV2}) band definitions using a handheld spectrometer at the Colville River Delta, Alaska, 2012–2015. The solid line through the origin represents the slope of a 1:1 relationship, and the dotted line represents the actual relationship $biomass_{observed}$ = 17.17 + 0.676($biomass_{predicted}$).

4.3. NDVI as a Phenology Metric

4.3.1. Seasonal Dynamics of NDVI and Percent Nitrogen

The shape of seasonal trends in NDVI varied annually for all NDVI variables, with median yearly peak values ranging from ~0.35 to 0.50 for eMO and from about 0.60 to 0.95 for spectrometer-derived NDVI variables (Figure 5A–C). In most years, all three NDVI curves tended to gently level off after their peak, but clear late-season declines occurred in both 2011 and 2015 (Figure 5A–C). There was no clear best fitting model that described eMODIS NDVI phenology, but seasonal NDVI patterns based on plot-scale measurements (SR_{WV2} and SR_{eMO}) were best described by lognormal curves (Table A1). The two spectrometer-derived NDVI variables followed similar seasonal trajectories, although SR_{WV2} curves had slightly lower amplitudes than SR_{eMO} in most years, and peaked several days later in 2012 and 2014 (Figure 5B,C).

Curves describing seasonal change in percent nitrogen also showed inter-annual variation. In all years, percent nitrogen peaked within two weeks of the beginning of data collection, and declined gradually over the course of the summer, before showing a slight increase around 8 August in most years (Figure 5D).

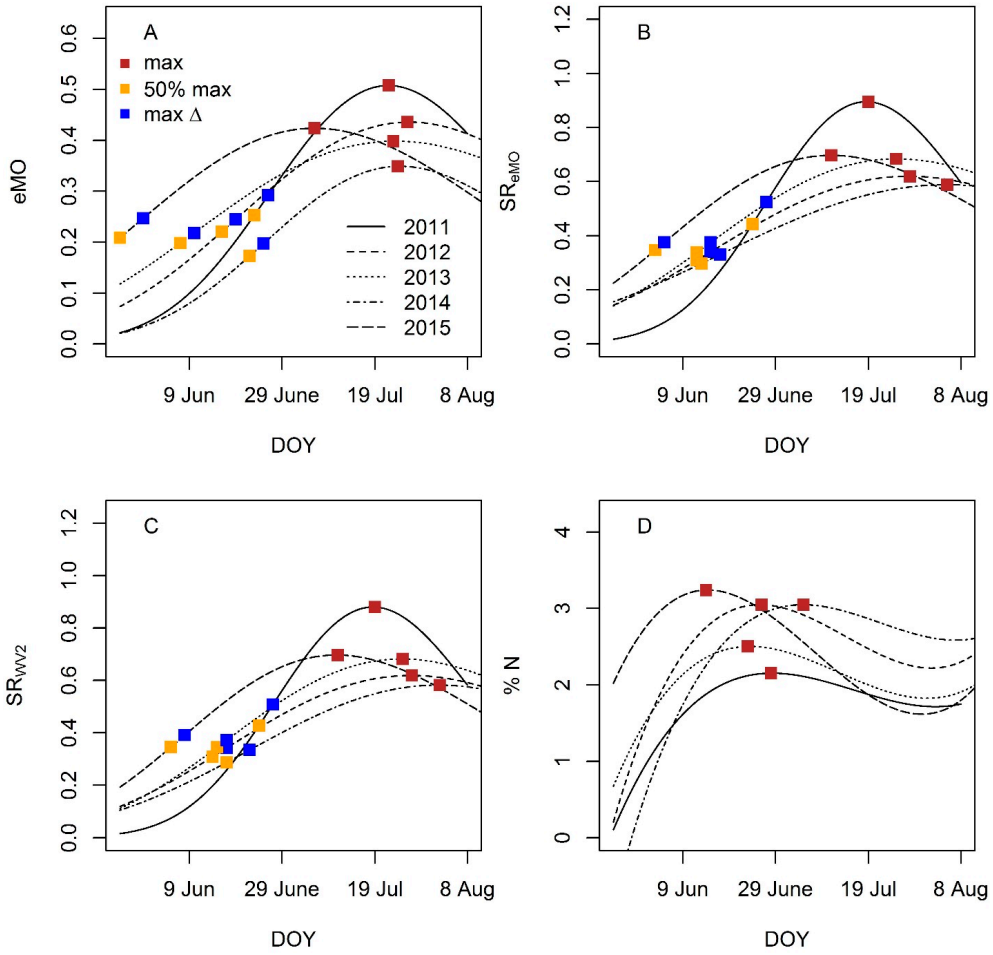

Figure 5. Seasonal trends in NDVI and percent nitrogen of halophytic graminoids at the Colville River Delta, Alaska, 2011–2015. Plots represent: (**A**) NDVI values derived from eMODIS satellite imagery (eMO); (**B**) NDVI values derived from handheld spectrometer using eMODIS band definitions (SR_{eMO}; (**C**) NDVI values derived from handheld spectrometer using Worldview-2 band definitions (SR_{WV2}); and (**D**) percent nitrogen in above-ground vegetation (%N). Metrics of NDVI phenology included date of maximum (max), half maximum (50% max), and maximum rate of change (max Δ). Annual seasonal trends for NDVI (**A**–**C**) were based on model-averaged predictions from Gaussian and lognormal non-linear regression while those for percent nitrogen (**D**) were based on a third-order polynomial. Dates are representative of non-leap years (i.e., 2011, 2013–2015).

4.3.2. Phenology Metric Estimation and Performance

There was substantial variability in the date of peak percent nitrogen among years (15 June–5 July; Figure 5D), which was predicted with different degrees of accuracy by each of the three phenology metrics (Figure 6). Overall, eMO predictions showed the strongest correlation with DOY of peak percent nitrogen. The two phenology metrics that were related to the timing of the early-season increase in NDVI, max Δ and 50% max, were both strong and significant predictors of interannual variation in date of peak percent nitrogen ($R^2 = 0.84$, $p < 0.02$; Figure 6A,D). In contrast, no phenology metric derived from spectrometer measurements of NDVI was a significant predictor of peak percent nitrogen at $\alpha \leq 0.05$ (Figure 6). The date of eMO 50% max occurred on average 3.4 days (range = 3–5 days) earlier than the date of eMO max Δ. When predicted peak percent nitrogen was regressed against observed dates, the slope of the relationship was slightly less than one for all phenology metrics and NDVI variables, but all models showed low average residual bias (Figure 6).

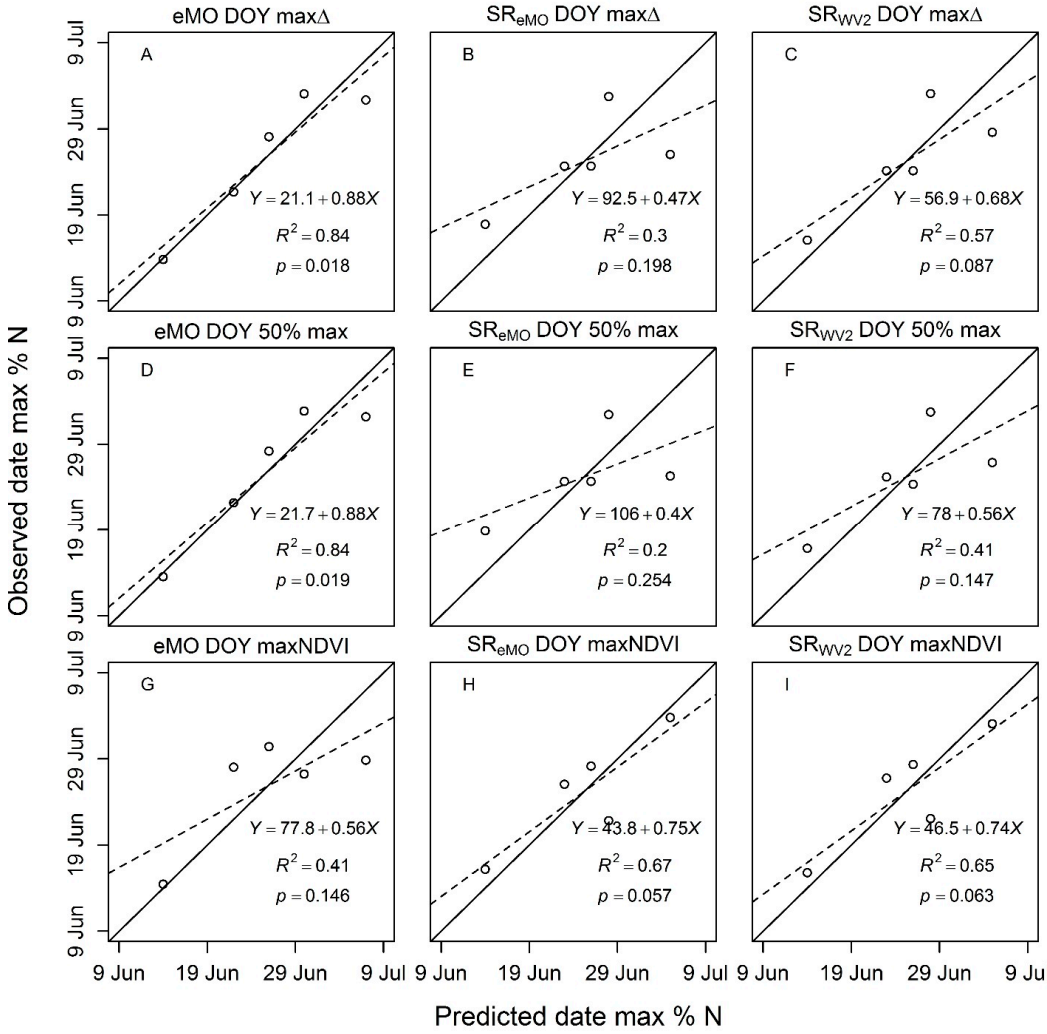

Figure 6. Comparisons of predicted and observed day of year (DOY) for peak nitrogen concentration (max %N) of halophytic graminoids across different NDVI phenology indices at the Colville River Delta, Alaska 2011–2015. NDVI phenology indices included DOY of maximum rate of change (DOY max Δ), half maximum (DOY 50% max), and maximum (max NDVI) and were generated from eMODIS satellite data (eMO), and handheld spectrometers with either eMODIS (SR_{eMO}) or Worldview2 (SR_{WV2}) band definitions. DOY of peak nitrogen was estimated by fitting 3rd-order polynomials to seasonal percent nitrogen measurements. Percent nitrogen predictions were generated from linear regression models of the general form (date peak vegetation %N ~β_0 + β_1x NDVI phenology index). Solid lines indicate a perfect 1:1 relationship, and dashed lines show the best fit lines from regression of predicted = β_0 + β_1x observed. Dates are representative of non-leap years (i.e., 2011, 2013–2015).

5. Discussion

5.1. NDVI as an Estimator of Biomass and Nitrogen

We found that the handheld spectrometer-derived NDVI was a useful estimator of seasonal changes in aboveground biomass and nitrogen biomass as measured in plots of *C. subspathacea*-dominated wetlands on the ACP. Models including measures of NDVI accounted for about 2/3 of the variance associated with spatial and temporal differences in biomass in these wetlands. Our results are consistent with those of Boelman et al. [25] who showed that handheld spectrometer-derived NDVI was a good estimator for biomass of freshwater graminoid wetlands located in the foothills of the ACP. Similarly, Hope et al. [26] found that the majority of the variation in NDVI readings was attributed to changes in biomass of ACP moist tussock and dry heath communities,

and Gamon, et al. [57] found that NDVI was strongly correlated with nitrogen mass per unit area across a variety of herbaceous and woody plant communities. Our fine (<1 m^2) scale assessment substantially outperformed the moderate (250 × 250 m) spatial resolution of the eMODIS-derived NDVI for assessing biomass of *C. subspathacea* within sample plots. Soil temperature, precipitation, and date variables were supported in our modeling approach, but predictions from models incorporating these variables differed minimally in average aboveground biomass (<2 g) from those including NDVI alone (Figure 3), indicating that spectrometer-derived NDVI alone was a good estimator for aboveground biomass. Although soil temperature and precipitation influence productivity of arctic tundra plants [29,48], NDVI appeared to capture most of the variation in plant biomass. Nevertheless, the strong correlation between NDVI and nitrogen biomass reflected the fact that nitrogen biomass and total biomass were highly correlated. As such, our models should not be used to infer correlation between NDVI and plant tissue percent nitrogen, which showed seasonal patterns distinct from those of NDVI and biomass.

The use of WorldView2 band definitions rather than eMODIS band definitions improved model performance for predicting biomass with our handheld spectrometer. These two band definitions were similar in their position and range in the red band but differed considerably in these definitions in the NIR band. Galvao et al. [58] showed that a NIR band that was placed at the shortest wavelength in the 750–1100 nm interval increased the NDVI contrast between green vegetation and senescent vegetation or soils. Given that clipped plots contained up to 20% of senescent plant material, we speculate that the lower position (WorldView2: 832 nm; eMODIS: 878 nm) and the wider range (WorldView2: 125 nm; eMODIS: 43 nm) of the NIR band for WorldView2 may have improved detection of live plants and increased accuracy of *C. subspathacea* biomass predictions in our study.

5.2. Sources of Error

Habitat heterogeneity at the larger scale of the eMODIS satellite-derived NDVI was likely a major reason for its poor performance (R^2 = 0.34–0.40) to predict seasonal changes in aboveground biomass. Halophytic wetlands were not uniformly distributed across the landscape and the 250 × 250 m footprint of the eMODIS spectral signal likely encompassed other communities with different plant species (e.g., freshwater graminoids, dwarf scrubs) and land cover types (i.e., water bodies, moist soils), thus reducing NDVI accuracy [25,26,35,39]. Further, satellite-derived spectral data is especially prone to degradation and alteration in the Arctic from frequent cloud cover, high sun angle, and suboptimal sun-object-sensor geometry that may affect NDVI values [59]. At the high resolution of the handheld spectrometer, small inter-plot differences in plant density and species composition may influence the NDVI values over the study period. But in our case, clipped plots were nearly exclusively (≥98%) *C. subspathacea*, therefore any errors associated in the spectral readings and biomass were likely associated with differentiating between live plants and dead material and moist soils.

The spatial scale of habitat heterogeneity is especially relevant in the context of our biomass validation exercise. We used spectrometer readings with Worldview2 band definitions to derive a model that predicted *C. subspathacea* biomass at the CRD. However, when we applied the same model to spectrometer readings in functionally similar stands of *C. subspathacea* at PL, biomass was overestimated by 25%. We suspect this positive bias was caused primarily by differences in plant characteristics between sites. Specifically, average biomass of *C. subspathacea* in plots at PL (98.5 g dry weight m^{-2}) were substantially higher than those at the CRD (68.0 g dry weight m^{-2}). Likewise, the associated NDVI values were also higher at PL (0.70) than at CRD (0.53). As such, biomass and NDVI values measured at PL occurred at the high end and outside the range of values derived for the predictive model at the CRD. Thus, although the NDVI model predicted biomass with an adequate degree of accuracy at the CRD, the positive bias in predicted values when applied at PL underscores the importance of site-specific validation when expanding the geographic scope of such models.

5.3. Ndvi as a Phenology Metric (Objective 2): Low Resolution Application

Compared to fine-scaled estimates obtained from the handheld spectrometer, the satellite-derived NDVI data provided more accurate estimates for the timing of peak nitrogen in *C. subspathacea*-dominated wetlands on the ACP (Figure 6). The timing of peak nitrogen concentration is an essential parameter for understanding reproductive success of arctic herbivores. Failure by an animal to adjust the timing of reproduction to match optimal availability of high quality food resources on breeding areas (i.e., "phenology mismatch") can lead to poor reproductive success [60–62], slower growth of young [61,63], and ultimately lower survival and recruitment [61,64,65]. The timing of peak nitrogen concentration in halophytic wetlands is not only important for assessing wildlife habitat quality, but is variable enough from year to year to require frequent monitoring. Our results show that this monitoring can be accomplished accurately and cost-effectively using publicly available satellite-derived NDVI products. Strong correlations between satellite NDVI and nitrogen phenology have also been demonstrated in moist non-acidic tundra communities of the High Arctic similar to the lower-quality freshwater graminoid wetlands near our study site [35], suggesting that our approach might be broadly applicable for monitoring nitrogen phenology in a wider range of arctic plant communities.

Beyond demonstrating the general applicability of NDVI as a tool to monitor the timing of peak nitrogen, our results also provide insight into how methodological choices influence model results. Some choices, like the selection of spectral band definitions for NDVI calculation, had little influence on the predictive power of NDVI phenology metrics. We also found that NDVI metrics related to the period of rapid spring growth (50% max and max Δ) were generally better indicators of nitrogen phenology than the date of peak NDVI, which is consistent with the idea that plants prioritize growth over structural stability during rapid early-season growth, resulting in low tissue C:N ratios. Furthermore, we demonstrated that 50% max was a reasonable approximation of max Δ (the period of peak spring green-up), which requires the ability to solve for the first derivative of a seasonal phenology curve. Previous studies have made, but not explicitly tested this assumption (e.g., [34,35]). Finally, and most surprisingly, we demonstrate that the use of a handheld spectrometer to measure NDVI at a finer spatial resolution did not result in better prediction of nitrogen phenology.

5.4. Performance of Satellite vs. Plot-Level NDVI Phenology Metrics

The strong performance of our eMODIS phenology models was counterintuitive because 250 × 250 m eMODIS pixels contained at least some water and non-target vegetation, including freshwater graminoid wetlands dominated by *Carex aquatilis*. As noted above, this heterogeneity likely contributed to the poor predictive power of linear models linking eMODIS NDVI to aboveground biomass, because NDVI-biomass relationships are specific to the vegetation type. However, common plant communities on the ACP show similar temporal trends in NDVI over the course of the growing season, with synchronous peaks in any given year [48]. Moreover, these trends have been shown to be correlated with regional average air and soil temperature patterns [48]. We suspect that eMODIS-derived phenology metrics may have been relatively insensitive to spatial heterogeneity in land cover within a pixel because all local vegetation types probably exhibited similar NDVI seasonality. If true, this suggests that our models linking NDVI to nitrogen phenology should be less site-specific than our models linking NDVI to biomass. However, because there were only two years of data from PL, we were unable to validate our inter-annual nitrogen phenology results with data from an independent site. Therefore, we caution against the extrapolation of our models to new study areas without estimating site-specific model parameters. In particular, NDVI-nitrogen phenology relationships could differ in areas at substantially higher or lower latitudes, where the duration and onset of the growing season are very different, or when the sampling period covers a different portion of the growing period. Although we anticipate that strong relationships between NDVI and nitrogen phenology would be detected in both scenarios, the shape of the best-fit curves defining seasonal trends in NDVI and nitrogen could be affected, resulting in biased estimates of peak nitrogen phenology.

An additional caveat to our results is that we do not have a definitive explanation for why eMODIS NDVI outperformed NDVI derived from the spectrometer as an estimator of nitrogen phenology. While local factors like soil properties can affect plot-scale biomass measurements [66], they may have little influence on seasonal nitrogen accumulation. In particular, localized grazing pressure could reduce the standing crop and therefore the NDVI value of any plot, yet previous research suggests that the effect of grazing on tissue nitrogen content in halophytic grazing wetlands is minimal for most of the growing season [67,68].

6. Conclusions

Our results support the use of plot-level NDVI derived from a handheld spectrometer as an alternative to intensive vegetation sampling as a means to monitor patterns in biomass, but only following site-specific validation. Satellite-derived NDVI shows promise for predicting seasonal timing of peak nitrogen, but both plot- and satellite-derived measures of NDVI were poor estimators of seasonal changes in nitrogen, demonstrating the need for alternative techniques to track this critical habitat parameter. Our study highlights the overall importance of matching the scale of NDVI measurements to the vegetation properties being studied (e.g., biomass vs. nitrogen phenology), and the scales at which those properties are regulated. Although previous studies have contrasted satellite and plot-scale NDVI as estimators of arctic vegetation biomass [2], we are unaware of other work that explicitly contrasts the predictive power of NDVI metrics for properties of vegetation across multiple scales. Given the current evidence for rapid changes in physical and environmental phenologyin the Arctic, conflicting consequences of a phenology mismatch between migratory herbivores and their food resources [69,70], and an interest in forecasting the future of plant forage quality and quantity for herbivores [6], there is a compelling need to improve monitoring of forage plant quantity and quality at high latitudes.

Acknowledgments: This research project is part of the U.S. Geological Survey (USGS) Changing Arctic Ecosystems Initiative supported by the USGS Ecosystems Mission Area, Wildlife Program. We especially thank Jaimlyn Korol, Jerrid Hixon, Cascade Gallasso-Irish, Tyrone Donnelly and Luke Burlingame for assistance with vegetation sampling at CRD and PL. In 2013 and 2014, the Colville River Delta project received funding for our interns through the USGS Student Interns in Support of Native American Relations Program and we are grateful for the support of the Arctic Slope Regional Corporation in securing these funds. ConocoPhillips Alaska, Inc. provided in-kind logistical support in all years. All data that support the findings of this publication can be found in [71]. Any use of trade, firm, or product names is for descriptive purposes only and does not imply endorsement by the U.S. Government.

Author Contributions: Kyle R. Hogrefe collected and managed the field data at the CRD, and wrote the initial draft manuscript. David H. Ward and Jerry W. Hupp led the research at CRP. Mike Budde provided eMODIS NDVI data and technical support. Daniel Ruthrauff and Vijay Patil provided analytical support for the manuscript. Brandt Meixell collected and managed field data at PL. All coauthors contributed to the text.

Conflicts of Interest: The authors declare no conflict of interest.

Appendix A

Table A1. Multi-model selection results for nonlinear curves used to predict seasonal patterns in NDVI and percent nitrogen in halophytic graminoids at the Colville River Delta, Alaska, 2011–2015. Results are derived from models fitted with all available data (pooled years) to show overall support for each curve function. eMODIS (eMO) model selection was based on a single pixel value for each date x year combination (n = 46). Spectrometer NDVI curves with eMODIS band definitions (SReMO) and WorldView 2 band definitions (SRWV2) were fit using measurements for all plots at all sampling dates in all years (n = 640). Lowest AIC_c scores: −108.71 (eMO), −1027.26 (SR_{eMO}), and −972.37 (SR_{WV2}).

Variable	Model	df	ΔAIC_c	ω_i
eMO	Gaussian	4	0.69	0.41
eMO	Lognormal	4	0.00	0.59
eMO	Null	2	27.61	0.00
SR_{eMO}	Gaussian	4	5.78	0.05
SR_{eMO}	Lognormal	4	0.00	0.95
SR_{eMO}	Null	2	322.43	0.00
SR_{WV2}	Gaussian	4	7.37	0.02
SR_{WV2}	Lognormal	4	0.00	0.98
SR_{WV2}	Null	2	348.13	0.00

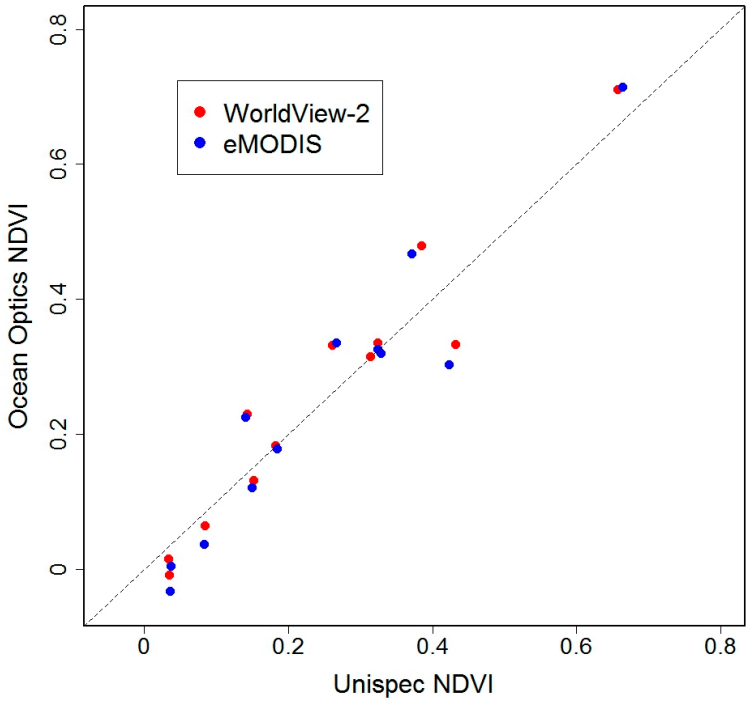

Figure A1. Comparison of NDVI values collected using two different handheld spectrometer units (OceanOptics and Unispec) with WorldView-2 (red) and eMODIS (blue) band definitions. Readings were collected at 12 plots representing a range of biomass values in halophytic graminoids. The dotted line through the origin represents the slope of a 1:1 relationship. Results of paired *t*-tests indicate that the units did not significantly differ in their readings (WorldView-2 t11 = 0.58, $p = 0.57$; eMODIS t11 = −0.05, $p = 0.96$).

References

1. Shaver, G.R.; Chapin, F.S. Production: Biomass relationships and element cycling in contrasting arctic vegetation types. *Ecol. Monogr.* **1991**, *61*, 1–31. [CrossRef]

2. Jia, G.J.; Epstein, H.E.; Walker, D.A. Greening of arctic alaska, 1981–2001. *Geophys. Res. Lett.* **2003**, *30*. [CrossRef]
3. Kittel, T.G.; Baker, B.B.; Higgins, J.V.; Haney, J.C. Climate vulnerability of ecosystems and landscapes on Alaska's north slope. *Reg. Environ. Chang.* **2011**, *11*, 249–264. [CrossRef]
4. Arp, C.D.; Jones, B.M.; Schmutz, J.A.; Urban, F.E.; Jorgenson, M.T. Two mechanisms of aquatic and terrestrial habitat change along an Alaskan arctic coastline. *Polar Biol.* **2010**, *33*, 1629–1640. [CrossRef]
5. Tape, K.D.; Flint, P.L.; Meixell, B.W.; Gaglioti, B.V. Inundation, sedimentation, and subsidence creates goose habitat along the arctic coast of Alaska. *Environ. Res. Lett.* **2013**, *8*, 045031. [CrossRef]
6. Van Hemert, C.; Flint, P.L.; Udevitz, M.S.; Koch, J.C.; Atwood, T.C.; Oakley, K.L.; Pearce, J.M. Forecasting wildlife response to rapid warming in the Alaskan Arctic. *BioScience* **2015**, *65*, 718–728. [CrossRef]
7. Ward, D.H.; Reed, A.; Sedinger, J.S.; Black, J.M.; Derksen, D.V.; Castelli, P.M. North American brant: Effects of changes in habitat and climate on population dynamics. *Glob. Chang. Biol.* **2005**, *11*, 869–880. [CrossRef]
8. Hupp, J.W.; Ward, D.H.; Hogrefe, K.R.; Sedinger, J.S.; Martin, P.D.; Stickney, A.A.; Obritschkewitsch, T. Growth of black brant and lesser snow goose goslings in northern Alaska. *J. Wildl. Manag.* **2017**, *81*, 846–857. [CrossRef]
9. Flint, P.L.; Mallek, E.J.; King, R.J.; Schmutz, J.A.; Bollinger, K.S.; Derksen, D.V. Changes in abundance and spatial distribution of geese molting near Teshekpuk Lake, Alaska: Interspecific competition or ecological change? *Polar Biol.* **2008**, *31*, 549–556. [CrossRef]
10. Burgess, R.M.; Ritchie, R.J.; Person, B.T.; Suydam, R.S.; Shook, J.E.; Prichard, A.K.; Obritschkewitsch, T. Rapid growth of a nesting colony of lesser snow geese (*Chen caerulescens caerulescens*) on the Ikpikpuk River delta, North Slope, Alaska, USA. *Waterbirds* **2017**, *40*, 11–23. [CrossRef]
11. Stehn, R.A.; Larned, W.W.; Platte, R.M. *Analysis of Aerial Survey Indices Monitoring Waterbird Populations of the Arctic Coastal Plain, Alaska, 1986–2012*; U.S. Fish and Wildlife Service: Anchorage, AK, USA, 2013.
12. Tucker, C.J. Spectral estimation of grass canopy variables. *Remote Sens. Environ.* **1977**, *6*, 11–26. [CrossRef]
13. Pettorelli, N.; Vik, J.O.; Mysterud, A.; Gaillard, J.M.; Tucker, C.J.; Stenseth, N.C. Using the satellite-derived NDVI to assess ecological responses to environmental change. *Trends Ecol. Evol.* **2005**, *20*, 503–510. [CrossRef] [PubMed]
14. Pettorelli, N.; Ryan, S.; Mueller, T.; Bunnefeld, N.; Jedrzejewska, B.; Lima, M.; Kausrud, K. The Normalized Difference Vegetation Index (NDVI): Unforeseen successes in animal ecology. *Clim. Res.* **2011**, *46*, 15–27. [CrossRef]
15. Hamel, S.; Garel, M.; Festa-Bianchet, M.; Gaillard, J.M.; Côté, S.D. Spring Normalized Difference Vegetation Index (NDVI) predicts annual variation in timing of peak faecal crude protein in mountain ungulates. *J. Appl. Ecol.* **2009**, *46*, 582–589. [CrossRef]
16. Garroutte, E.L.; Hansen, A.J.; Lawrence, R.L. Using NDVI and EVI to map spatiotemporal variation in the biomass and quality of forage for migratory elk in the greater Yellowstone ecosystem. *J. Remote Sens.* **2016**, *8*, 404. [CrossRef]
17. Tucker, C.J.; Vanpraet, C.L.; Sharman, M.J.; Van Ittersum, G. Satellite remote sensing of total herbaceous biomass production in the Senegalese Sahel: 1980–1984. *Remote Sens. Environ.* **1985**, *17*, 233–249. [CrossRef]
18. Pedersen, A.O.; Jepsen, J.U.; Yoccoz, N.G.; Fuglei, E. Ecological correlates of the distribution of territorial Svalbard rock ptarmigan. *Can. J. Zool.* **2007**, *85*, 122–132. [CrossRef]
19. Mallegowda, P.; Grengaian, G.; Krishnan, J.; Niphadkar, M. Assessing habitat quality of forest-corridors through NDVI analysis in dry tropical forests of south India: Implications for conservation. *J. Remote Sens.* **2015**, *7*, 1619–1639. [CrossRef]
20. Zhou, L.; Kaufmann, R.K.; Myneni, R.B.; Tucker, C.J. Relation between interannual variations in satellite measures of northern forest greenness and climate between 1982 and 1999. *J. Geophys. Res.* **2003**, *108*, 4004. [CrossRef]
21. Pettorelli, N. *The Normalized Difference Vegetation Index*; Oxford University Press: Oxford, UK, 2013.
22. Asrar, G.; Fuchs, M.; Kanemasu, E.T.; Hatfield, J.L. Estimating absorbed photosynthetic radiation and leaf area index from spectral reflectance in wheat. *Agron. J.* **1984**, *76*, 300–306. [CrossRef]
23. Sellers, P.J. Canopy reflectance, photosynthesis and transpiration. *Int. J. Remote Sens.* **1985**, *6*, 1335–1372. [CrossRef]
24. Myneni, R.B.; Hall, F.G.; Sellers, P.J.; Marshak, A.L. The interpretation of spectral vegetation indexes. *IEEE Trans. Geosci. Remote Sens.* **1995**, *33*, 481–486. [CrossRef]

25. Boelman, N.T.; Stieglitz, M.; Rueth, H.M.; Sommerkorn, M.; Griffin, K.L.; Shaver, G.R.; Gamon, J.A. Response of NDVI, biomass, and ecosystem gas exchange to long-term warming and fertilization in wet sedge tundra. *Oecologia* **2003**, *135*, 414–421. [CrossRef] [PubMed]
26. Hope, A.S.; Kimball, J.S.; Stow, D.A. The relationship between tussock tundra spectral reflectance properties and biomass and vegetation composition. *Int. J. Remote Sens.* **1993**, *14*, 1861–1874. [CrossRef]
27. Boelman, N.T.; Stieglitz, M.; Griffin, K.L.; Shaver, G.R. Inter-annual variability of NDVI in response to long-term warming and fertilization in wet sedge and tussock tundra. *Oecologia* **2005**, *143*, 588–597. [CrossRef] [PubMed]
28. Boelman, N.T.; Gough, L.; McLaren, J.R.; Greaves, H. Does NDVI reflect variation in the structural attributes associated with increasing shrub dominance in arctic tundra? *Environ. Res. Lett.* **2011**, *6*, 035501. [CrossRef]
29. Raynolds, M.K.; Walker, D.A.; Verbyla, D.; Munger, C.A. Patterns of change within a tundra landscape: 22-year landsat NDVI trends in an area of the northern foothills of the Brooks Range, Alaska. *Arct. Antarct. Alp. Res.* **2013**, *45*, 249–260. [CrossRef]
30. Han, S.; Hendrickson, L.L.; Ni, B. Comparison of satellite and aerial imagery for detecting leaf chlorophyll content in corn. *Trans. ASAE* **2002**, *45*, 1229–1236.
31. Blackmer, T.M.; Schepers, J.S. Use of a chlorophyll meter to monitor nitrogen status and schedule fertization for corn. *J. Prod. Agric.* **1995**, *8*, 56–60. [CrossRef]
32. Myneni, R.B.; Keeling, C.; Tucker, C.J.; Asrar, G.; Nemani, R.R. Increased plant growth in the northern high latitudes from 1981 to 1991. *Nature* **1997**, *386*, 698–702. [CrossRef]
33. Karlsen, S.; Elvebakk, A.; Høgda, K.; Grydeland, T. Spatial and temporal variability in the onset of the growing season on Svalbard, arctic Norway—Measured by modis-NDVI satellite data. *Remote Sens.* **2014**, *6*, 8088–8106. [CrossRef]
34. Griffith, B.; Douglas, D.C.; Walsh, N.E.; Young, D.D.; McCabe, T.R.; Russell, D.E.; White, R.G.; Cameron, R.D.; Whitten, K.R. The porcupine caribou herd. In *Arctic Refuge Coastal Plain Terrestrial Wildlife Research Summaries*; Douglas, D.C., Reynolds, P.E., Rhode, E.B., Eds.; U.S. Geological Survey, Biological Resources Division: Springfield, VA, USA, 2002; pp. 8–37.
35. Doiron, M.; Legagneux, P.; Gauthier, G.; Lévesque, E. Broad-scale satellite normalized difference vegetation index data predict plant biomass and peak date of nitrogen concentration in arctic tundra vegetation. *Appl. Veg. Sci.* **2013**, *16*, 343–351. [CrossRef]
36. Bhatt, U.S.; Walker, D.A.; Raynolds, M.K.; Comiso, J.C.; Epstein, H.E.; Jia, G.; Gens, R.; Pinzon, J.E.; Tucker, C.J.; Tweedie, C.E. Circumpolar arctic tundra vegetation change is linked to sea ice decline. *Earth Interact.* **2010**, *14*, 1–20. [CrossRef]
37. Bhatt, U.S.; Walker, D.A.; Raynolds, M.K.; Bieniek, P.A.; Epstein, H.E.; Comiso, J.C.; Pinzon, J.E.; Tucker, C.J.; Polyakov, I.V. Recent declines in warming and vegetation greening trends over pan-arctic tundra. *Remote Sens.* **2013**, *5*, 4229–4254. [CrossRef]
38. Bieniek, P.A.; Bhatt, U.S.; Walker, D.A.; Raynolds, M.K.; Comiso, J.C.; Epstein, H.E.; Pinzon, J.E.; Tucker, C.J.; Thoman, R.L.; Tran, H. Climate drivers linked to changing seasonality of alaska coastal tundra vegetation productivity. *Earth Interact.* **2015**, *19*, 1–29. [CrossRef]
39. Huete, A.; Didan, K.; Miura, T.; Rodriguez, E.P.; Gao, X.; Ferreira, L.G. Overview of the radiometric and biophysical performance of the modis vegetation indices. *Remote Sens. Environ.* **2002**, *83*, 195–213. [CrossRef]
40. Myneni, R.; Asrar, G. Atmospheric effects and spectral vegetation indices. *Remote Sens. Environ.* **1994**, *47*, 390–402. [CrossRef]
41. Person, B.T.; Herzog, M.P.; Ruess, R.W.; Sedinger, J.S.; Anthony, R.M.; Babcock, C.A. Feedback dynamics of grazing lawns: Coupling vegetation change with animal growth. *Oecologia* **2003**, *135*, 583–592. [CrossRef] [PubMed]
42. Viereck, L.A.; Dyrness, C.; Batten, A.; Wenzlick, K. *The Alaska Vegetation Classification*; U.S. Department of Agriculture, Forest Service, Pacific Northwest Research Station: Portland, OR, USA, 1992.
43. Brown, J.; Howard, D.; Wylie, B.; Frieze, A.; Ji, L.; Gacke, C. Application-ready expedited modis data for operational land surface monitoring of vegetation condition. *Remote Sens.* **2015**, *7*, 16226–16240. [CrossRef]
44. Jenkerson, C.; Maiersperger, T.; Schmidt, G. *Emodis: A User-Friendly Data Source*; 2331–1258; U.S. Geological Survey: Reston, VA, USA, 2010.

45. Swets, D.L.; Reed, B.C.; Rowland, J.D.; Marko, S.E. A weighted least-squares approach to temporal NDVI smoothing. In Proceedings of the ASPRS Annual Conference: From Image to Information, Portland, OR, USA, 17–21 May 1999.
46. Burnham, K.P.; Anderson, D.R. *Model Selection and Multimodel Inference: A Practical Information-Theoretic Approach*; Springer Science & Business Media: Berlin, Germany, 2003.
47. Pinheiro, J.C.; Bates, D.M. Linear mixed-effects models: Basic concepts and examples. In *Mixed-Effects Models in S and S-Plus*; Springer: New York, NY, USA, 2000.
48. Jia, G.J.; Epstein, H.E.; Walker, D.A. Controls over intra-seasonal dynamics of avhrr NDVI for the arctic tundra in northern Alaska. *Int. J. Remote Sens.* **2004**, *25*, 1547–1564. [CrossRef]
49. Team, R.C. *R: A Language and Environment for Statistical Computing (Version 3.1.4)*; R Foundation for Statistical Computing: Vienna, Austria, 2014.
50. Bates, D.; Maechler, M.; Bolker, B.; Walker, S.; Christensen, R.; Singmann, H.; Dai, B.; Grothendieck, G. Package "lme4". R Package Version 1.1–10. Available online: http://lme4.R-forge.R-project.Org/ (accessed on 15 March 2017).
51. Mazerolle, M.J. Aiccmodavg: Model Selection and Multimodel Inference Based on (q) aic (c). R Package Version 2.1-0. Available online: http://CRAN.R-project.org/package=AICcmodavg (accessed on 15 March 2017).
52. Knowles, J.; Frederick, C. Mertools: Tools for Analyzing Mixed Effect Regression Models [r Package Version 0.3.0]. R Package Version 0.3.0. Available online: http://CRAN.R-project.org/package=merTools (accessed on 15 March 2017).
53. Nakagawa, S.; Schielzeth, H. A general and simple method for obtaining r2 from generalized linear mixed-effects models. *Methods Ecol. Evol.* **2013**, *4*, 133–142. [CrossRef]
54. Lefcheck, J.S. Piecewisesem: Piecewise Structural Equation Modeling. R Package Version 1.2.1. Available online: http://CRAN.R-project/package=piecewiseSEM (accessed on 15 March 2017).
55. Chapin, F.S., III; Van Cleve, K.; Tieszen, L. Seasonal nutrient dynamics of tundra vegetation at Barrow, Alaska. *Arct. Alp. Res.* **1975**, *7*, 209–226.
56. Elzhov, T.; Mullen, K.; Spiess, A.; Bolker, B. *Minpack. Lm: R Interface to the Levenberg-Marquardt Nonlinear Least-Squares Algorithm Found in Minpack, Plus Support for Bounds*; (ver. 1.2-0) r Package, 1.2-1; The Comprehensive R Archive Network (CRAN): Vienna, Austria, 2015.
57. Gamon, J.A.; Field, C.B.; Goulden, M.L.; Griffin, K.L.; Hartley, A.E.; Joel, G.; Penuelas, J.; Valentini, R. Relationships between NDVI, canopy structure, and photosynthesis in three californian vegetation types. *Ecol. Appl.* **1995**, *5*, 28–41. [CrossRef]
58. Galvao, L.S.; Vitorello, I.; Pizarro, M.A. An adequate band positioning to enhance NDVI contrasts among green vegetation, senescent biomass, and tropical soils. *Int. J. Remote Sens.* **2000**, *21*, 1953–1960. [CrossRef]
59. Buchhorn, M.; Raynolds, M.K.; Walker, D.A. Influence of brdf on NDVI and biomass estimations of alaska arctic tundra. *Environ. Res. Lett.* **2016**, *11*, 125002. [CrossRef]
60. Stevenson, I.R.; Bryant, D.M. Avian phenology: Climate change and constraints on breeding. *Nature* **2000**, *406*, 366–367. [CrossRef] [PubMed]
61. Brook, R.; Leafloor, J.; Abraham, K.; Douglas, D. Density dependence and phenological mismatch: Consequences for growth and survival of sub-arctic nesting Canada geese. *Avian Conserv. Ecol.* **2015**, *10*, 1. [CrossRef]
62. Ross, M.V.; Alisauskas, R.T.; Douglas, D.C.; Kellett, D.K. Decadal declines in avian herbivore reproduction: Density-dependent nutrition and phenological mismatch in the Arctic. *Ecology* **2017**, *98*, 1869–1883. [CrossRef] [PubMed]
63. McKinnon, L.; Picotin, M.; Bolduc, E.; Juillet, C.; Bêty, J. Timing of breeding, peak food availability, and effects of mismatch on chick growth in birds nesting in the high Arctic. *Can. J. Zool.* **2012**, *90*, 961–971. [CrossRef]
64. Post, E.; Forchhammer, M.C. Climate change reduces reproductive success of an arctic herbivore through trophic mismatch. *Philos. Trans. R. Soc. Lond. B Biol. Sci.* **2008**, *363*, 2367–2373. [CrossRef] [PubMed]
65. Sedinger, J.S.; Flint, P.L.; Lindberg, M.S. Environmental influence on life-history traits: Growth, survival, and fecundity in black brant (*branta bernicla*). *Ecology* **1995**, *76*, 2404–2414. [CrossRef]
66. Schuur, E.A.; Crummer, K.G.; Vogel, J.G.; Mack, M.C. Plant species composition and productivity following permafrost thaw and thermokarst in alaskan tundra. *Ecosystems* **2007**, *10*, 280–292. [CrossRef]

67. Zellmer, I.; Clauss, M.; Hik, D.; Jefferies, R. Growth responses of arctic graminoids following grazing by captive lesser snow geese. *Oecologia* **1993**, *93*, 487–492. [CrossRef] [PubMed]
68. Hik, D.; Sadul, H.; Jefferies, R. Effects of the timing of multiple grazings by geese on net above-ground primary production of swards of *puccinellia phryganodes*. *J. Ecol.* **1991**, *71*, 715–730. [CrossRef]
69. Post, E.; Forchhammer, M.C.; Bret-Harte, M.S.; Callaghan, T.V.; Christensen, T.R.; Elberling, B.; Fox, A.D.; Gilg, O.; Hik, D.S.; Høye, T.T. Ecological dynamics across the Arctic associated with recent climate change. *Science* **2009**, *325*, 1355–1358. [CrossRef] [PubMed]
70. Gustine, D.; Barboza, P.; Adams, L.; Griffith, B.; Cameron, R.; Whitten, K. Advancing the match-mismatch framework for large herbivores in the Arctic: Evaluating the evidence for a trophic mismatch in caribou. *PLoS ONE* **2017**, *12*, e0171807. [CrossRef] [PubMed]
71. Normalized Difference Vegetation Index, Biomass and Nitrogen Concentration of Goose Forage, Arctic Coastal Plain, Alaska, 2011–2015; U.S. Geological Survey data release, 2017. [CrossRef]